coatings

MDPI

Article

Enhanced Electrical Properties and Stability of P-Type Conduction in ZnO Transparent Semiconductor Thin Films by Co-Doping Ga and N

Chien-Yie Tsay * and Wan-Yu Chiu

Department of Materials Science and Engineering, Feng Chia University, Taichung 40724, Taiwan; Chiuwanyu@gmail.com

* Correspondence: cytsay@mail.fcu.edu.tw; Tel.: +886-4-2451-7250 (ext. 5312)

Received: 20 October 2020; Accepted: 2 November 2020; Published: 6 November 2020

Abstract: P-type ZnO transparent semiconductor thin films were prepared on glass substrates by the sol-gel spin-coating process with N doping and Ga–N co-doping. Comparative studies of the microstructural features, optical properties, and electrical characteristics of ZnO, N-doped ZnO (ZnO:N), and Ga–N co-doped ZnO (ZnO:Ga–N) thin films are reported in this paper. Each as-coated sol-gel film was preheated at 300 °C for 10 min in air and then annealed at 500 °C for 1 h in oxygen ambient. X-ray diffraction (XRD) examination confirmed that these ZnO-based thin films had a polycrystalline nature and an entirely wurtzite structure. The incorporation of N and Ga–N into ZnO thin films obviously refined the microstructures, reduced surface roughness, and enhanced the transparency in the visible range. X-ray photoelectron spectroscopy (XPS) analysis confirmed the incorporation of N and Ga–N into the ZnO:N and ZnO:Ga–N thin films, respectively. The room temperature PL spectra exhibited a prominent peak and a broad band, which corresponded to the near-band edge emission and deep-level emission. Hall measurement revealed that the ZnO semiconductor thin films were converted from n-type to p-type after incorporation of N into ZnO nanocrystals, and they had a mean hole concentration of 1.83×10^{15} cm^{-3} and a mean resistivity of 385.4 Ω·cm. In addition, the Ga–N co-doped ZnO thin film showed good p-type conductivity with a hole concentration approaching 4.0×10^{17} cm^{-3} and a low resistivity of 5.09 Ω·cm. The Ga–N co-doped thin films showed relatively stable p-type conduction (>three weeks) compared with the N-doped thin films.

Keywords: p-type oxide semiconductor; ZnO thin film; N doping; Ga–N co-doping; sol-gel spin coating; electrical stability

1. Introduction

Wide-bandgap oxide semiconductors have gained considerable attention and received great interest due to their potential for applications in optoelectronic devices, photovoltaic devices, and transparent oxide electronics, such as ultraviolet photodetectors, short wavelength light-emitting diodes, thin-film solar cells, transparent resistive random access memory, and transparent field-effect transistors [1–4]. The fabrication of light-emitting diodes, p-n junction photodetectors, and complementary metal-oxide-semiconductor devices requires the combination of both n-type and p-type oxide semiconductors. The lack of availability of stable p-type oxide semiconductors limits the electrical efficiency of p-n junction-based devices or bipolar device applications [3,5]. Therefore, the development of stable and reproducible p-type oxide semiconductor thin films is necessary.

The crystalline wurtzite ZnO exhibits n-type conductivity due to a deviation from chemical stoichiometry and the presence of native point defects such as O vacancies (Vo) and Zn interstitials (Zn_i)

that makes the electrons easily be excited to the conduction band [2,6]. The difficulty in achieving p-type ZnO semiconductors is caused by a combination of deep acceptor levels, the low solubility of acceptors, and a strong self-compensation effect [7,8]. Previous studies demonstrated that the impurity doping of ZnO is an important approach for modulating the carrier concentration and electrical resistivity to satisfy device applications [9,10]. A sufficient amount of acceptors should be generated to overcome the n-type back ground, such as any donor-like defects created through preparation processes. It has been suggested that the group V element nitrogen (N) may be a potential acceptor dopant for O site substitution in ZnO to obtain p-type conductivity, for N has the smallest ionization energy among the group V dopants (N, P, and As) [2,11]. In addition, N (0.146 nm) and O (0.140 nm) have close ionic radii, and so N ions may easily be substituted on O sites of the ZnO lattice [12]. Moreover, the N–O bond length (1.88 Å) is close to the Zn–O bond length (1.93 Å) [13]. Kim's group reported that the incorporation of N as a dopant changed the conductivity of sol-gel-derived ZnO thin films from n-type to p-type and produced ZnO:N thin films with a hole concentration of 8.11×10^{16} cm^{-3} when the N doping content reached 20 at.% in the resultant solution [14]. However, the production of device-quality p-type conduction in N-doped ZnO thin films remains a challenge due to the low dopant solubility in the host material and high ionization energy [11].

Co-doping of two kinds of extrinsic atoms (using acceptors and donors simultaneously) is considered an effective method for producing stable p-type conductivity in ZnO semiconductor thin films [7,15,16]. Previous experimental studies found that acceptor and donor co-doped ZnO thin films not only exhibited p-type conductivity but also showed reasonable stability and reproducibility in electrical characteristics [17–19]. It was reported that simultaneous doping of nitrogen and group III elements can improve the hole concentration and enhance the stability of p-type ZnO thin film because the doping of the reactive donor element increases the solubility of nitrogen in ZnO [20–23]. According to first-principles calculations, Yan et al. proposed that the formation of passive acceptor-donor (Ga–N) complexes can create an impurity band above the valence-band maximum (VBM) in ZnO crystal based on reduction of the ionization energies of dopants [8]. A theoretical study by Duan et al. reported that the ionization energy of Ga–2N complex is lower than that of the single N acceptor [11]. The generation of N–Ga–N complexes could increase the solubility percentage of N ionized dopants and achieve shallower acceptor levels [6]. A previous report noted that the co-doping of Ga and N in ZnO thin films achieved the best p-type character among the types of impurity co-doped ZnO thin films [8]. Theoretical calculations also predict that Ga–N co-doped ZnO would yield better p-type conduction than Al–N co-doped ZnO [11]. This prediction is consistent with numerous experimental finding.

Several thin film deposition techniques have been employed to produce the group III (B, Al, Ga, and In)–N co-doped p-type ZnO semiconductor thin films including chemical vapor deposition, molecular-beam epitaxy, pulsed laser deposition, radio-frequency (rf) magnetron sputtering, spray pyrolysis, and the sol-gel method [2,7]. Most researchers have focused on the preparation of p-type ZnO thin films and investigated the effects of acceptor-donor co-doping on the physical properties. The authors noted that few studies have reported the electrical stability of solution-processed p-type ZnO thin films. There is no report on Ga–N co-doping p-type ZnO thin films prepared by the sol-gel method. Therefore, we prepared ZnO, ZnO:N, and ZnO:Ga–N thin films on glass substrates via the sol-gel method and spin-coating technique. The structural-physical properties relation of ZnO-based semiconductor thin films was investigated in detail through variation of the structural features to examine if they affect the optical properties and electrical characteristics. In addition, the electrical stability of p-type ZnO-based thin films was verified and is reported in this study.

2. Materials and Methods

2.1. Coating Solution Synthesis and Thin Film Deposition

The series of ZnO-based thin films, including undoped ZnO, N-doped ZnO (ZnO:N), and N–Ga co-doped ZnO (ZnO:N–Ga), were deposited on alkali-free glass substrates (Nippon Electric Glass

OA-10, 50 × 50 × 0.7 mm^3 in size) using the sol-gel method and spin coating technique. Prior to the deposition of the thin films, the glass substrates were ultrasonically cleaned in detergent, isopropyl alcohol, and acetone, washed thoroughly with distilled water and dried on a hot plate at 110 °C for 15 min. Three kinds of analytical reagent (AR)-grade metallic salts, including zinc acetate dihydrate ($Zn(CH_3CO_2)_2{\cdot}2H_2O$, J.T. Baker, Phillipsburg, NJ, USA), ammonium acetate (CH_3COONH_4, Sigma, St. Louis, MO, USA), and gallium (III) nitrate hydrate ($Ga(NO_3)_3{\cdot}xH_2O$, Alderich, St. Louis, MO, USA), were chosen as the source materials of zinc, nitrogen, and gallium, respectively. The first precursor solutions were synthesized by dissolving a stoichiometric ratio of AR-grade metallic salts in 2-methoxyethanol (solvent) and diethanolamine (stabilizing agent) using a stirring hot plate (PC-420D, Corning, Glendale, AZ, USA) at 60 °C for 2 h until the resultant solution became clear and transparent. After that procedure, the synthesized sols were aged for 72 h at room temperature under atmospheric environment before being used in the spin-coating process. The concentration of the amount of metal ions in the resultant solutions was maintained at 0.4 M [24] and the molar ratio of metal ions to stabilizing agent was kept at 1:1. In addition, the atomic ratio of [N]/[Zn + N] was 0.3 for two impurity doped thin films (ZnO:N and ZnO:N–Ga), and that of [Ga]/[Zn + N] was 0.01 for ZnO:N–Ga thin films. The respective sols were spin coated on the pre-cleaned glass substrates at 1000 rpm for 30 s, followed by preheating at 300 °C in air for 10 min to evaporate volatile materials. That procedure was repeated three times, and then the dried sol-gel films were annealed at 500 °C in oxygen ambient for 1 h to remove residual organic compounds of the gel films and achieve crystalline oxide thin films [22].

2.2. Characterization Techniques

The crystalline structure and crystallinity of the as-prepared ZnO-based thin films were analyzed by Bruker D8 Discover SSS high-resolution X-ray diffractometer (XRD, Bruker, Karlsruhe, Germany) with Cu-Kα radiation (λ = 1.5418 Å) by glancing incidence technique at an incident angle of 0.8°. Plane-view and cross-sectional view micrographs of the thin film samples were acquired by Hitachi S-4800 field-emission scanning electron microscope (FE-SEM, Hitachi, Tokyo, Japan). A Digital Instrument scanning probe microscope (SPM, NS4/D3100CL/MultiMode, Digital Instrument, Mannheim, Germany) was employed for characterizing the surface morphology and surface roughness of oxide films in tapping mode with a tip scanning rate of 0.7 Hz. The chemical bonding energies and elemental composition of the oxide films were determined by X-ray photoelectron spectroscopy (XPS, ULVAC-PHI PHI 5000 VersaProbe, Kanagawa, Japan). Prior to the XPS examination, Ar ion sputter-etching was performed for 15 s to remove the surface contamination. The optical transmission characteristics of the samples of glass/ZnO-based thin films were examined with a Hitachi U-2900 ultraviolet-visible (UV-Vis) spectrophotometer (Hitachi, Tokyo, Japan). Room-temperature (RT) emission spectra of three ZnO-based thin films were measured by the HORIBA Jobin Yvon photoluminescence (PL) spectrometer (LabRAM HR, Paris, France) with an excitation wavelength of 325 nm. The electrical characteristics of each thin film sample were measured by the van der Pauw method using the Hall-effect measurement system (HMS-3000, Ecopia, Gyeonggi-do, Korea) with a magnetic field of 0.55 T at RT.

3. Results and Discussion

Various types of nitrogen (N) sources, including NH_3, N_2, NO, N_2O, and CH_3COONH_4 have been successfully used to prepare of device-quality p-type ZnO semiconductor thin films. In this study, the N dopant was obtained through decomposition of ammonium acetate to acetamide and then to CO, NO, and NO_2 [24]. The NO and NO_2 acted as the N sources. It was suggested that NO easily forms N_O acceptors, which are shallow acceptors in ZnO [2,8]. Moreover, it was necessary to provide oxygen to suppress oxygen vacancy (Vo) formation during the preparation of solution-processed p-type ZnO thin films. Because Vo may form as a compensation center in p-type ZnO [25], we performed the post deposition crystallization heat treatment in pure oxygen atmosphere to decrease the background carrier concentration.

The results of the XRD examination, shown in Figure 1, indicate that the three kinds of ZnO-based thin films were polycrystalline in nature. The intense sharp diffraction peaks suggested that the pure ZnO thin film had better crystallinity (pattern (i) in Figure 1) than those of the two impurity-doped ZnO thin films. Previous studies reported that the crystalline quality of oxide thin films would be degraded by impurity doping [10,26,27]. Comparison of collected XRD patterns (in 2θ range from 25° to 65°) with the standard JCPDS file of ZnO crystal (JCPDS No. 36-1451) indicated the hexagonal wurtzite phase in the ZnO-based thin films. In addition, no X-ray diffraction signals related to other crystal phases, such as GaN, Ga_2O_3, and Zn_3N_2, were detected from the set of thin film samples, indicating the formation of a single phase.

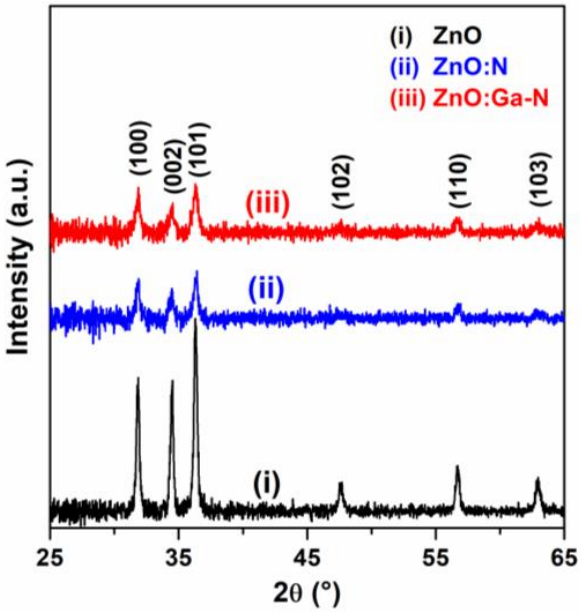

Figure 1. X-ray diffraction (XRD) patterns of ZnO, N-doped ZnO (ZnO:N), and Ga–N co-doped ZnO (ZnO:Ga–N) thin films deposited on glass substrates by the sol-gel spin-coating process.

A preferential orientation may occur due to nucleation, horizontal growth of the nuclei and vertical growth of the closed layer. As shown in Figure 1, we not only confirmed that these as-prepared ZnO thin films had a predominance of hexagonal wurtzite phase but also observed that they achieved a favorable orientation along the (101) plane. The relative intensities of $I_{(101)}/I_{(1000)\,+\,(002)\,+\,(101)}$ for the ZnO, ZnO:N, and ZnO:Ga–N samples were 0.422, 0.406, and 0.387, respectively. The calculated results reveal that the relative diffraction intensity of the undoped sample (0.422) was significantly smaller than that of the relative intensity (0.497) obtained from the standard JCPDS database; incorporation of N and Ga–N into the ZnO changed the growth rate of the (101) plane such that the three main diffraction planes had close growth rates. It is noted that the diffraction signals of the (102) and (103) planes were very weak for the two impurity-doped samples, implying an apparent decrease in crystallinity. According to the above discussion, we found that these sol-gel-derived ZnO-based thin films had no preferential orientation; impurity doping favored random growth of crystallites and caused degradation of the crystallinity. The average crystallite sizes of the thin film samples were quantified from the full widths at half-maximum and the Bragg diffraction angles of the three major diffraction peaks, (100), (002), and (101), with Scherrer's formula and are presented in Table 1. Table 1 summarizes our examined and calculated results on the structural features and optical properties. The average crystallite sizes for the undoped, N doped and Ga–N co-doped ZnO thin films were 26.9, 20.4, and 17.0 nm, respectively. It was determined that all the obtained ZnO-based thin films consisted of nanocrystals; N doping significantly inhibited the crystal growth rate due to lattice distortion, and the Zn:Ga–N samples had the smallest average crystallite size.

Table 1. Microstructural features and optical parameters of the obtained ZnO-based thin films.

Sample	Average Crystallite Size (nm)	Root Mean Square (RMS) Roughness (nm)	Average Transmittance [a] (%)	Absorption Reflectance [b] (cm^{-1})	Optical Bandgap (eV)	Urbach Energy (meV)
ZnO	26.9	3.6	85.14	19,019	3.27	89.2
ZnO:N	20.4	2.7	89.77	24,020	3.24	123.8
ZnO:Ga–N	17.0	1.1	90.29	25,574	3.24	148.5

The average transmittance values [a] and average absorption coefficients [b] were calculated from the recorded transmittance data of wavelengths from 400 to 800 nm.

Figure 2 shows the cross-sectional FE-SEM micrographs of ZnO-based thin films deposited onto glass substrates, which revealed good thickness uniformity. It can be seen that these oxide thin films possessed significantly granular microstructures, had homogeneous particle size distributions, and exhibited nano-sized pores inside the sol-gel-derived ZnO-based thin films. In addition, it was significantly observed that the mean particle size of the N-doped thin film was smaller than that of the undoped thin film, and the Ga–N co-doped thin film possessed the finest grade of particles. The microstructural features of the developed thin films, observed by FE-SEM, were consistent with the results of the XRD examination. The thickness of each thin film sample was estimated from the corresponding cross-sectional FE-SEM micrograph. The mean film thicknesses of the undoped, N-doped, and Ga–N co-doped ZnO thin films were found to be 85, 45, and 40 nm, respectively. The difference in film thickness between the three kinds of ZnO-based thin films can be ascribed to the variation in the viscosities of the coating solutions with the concentration of solute (metallic salts). The corresponding plane-view FE-SEM micrographs are shown in Figure S1. In that figure, it is clearly shown that the free surfaces of the films were flat, with no visible pores or cracks in the observation area.

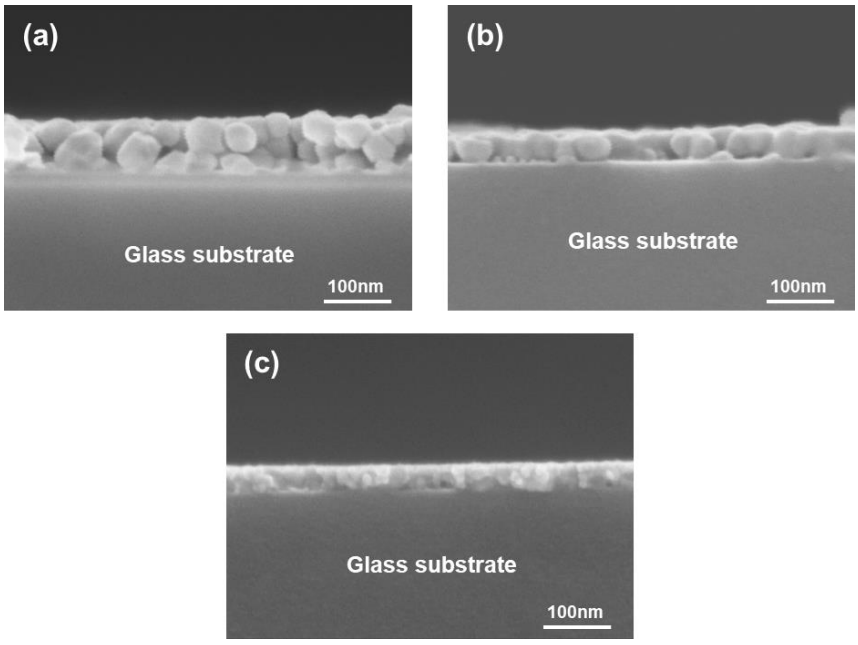

Figure 2. Cross-sectional field-emission scanning electron microscope (FE-SEM) micrographs of ZnO-based thin films: (**a**) undoped, (**b**) N-doped, and (**c**) Ga–N co-doped samples.

The topographic features of each thin film sample were examined by SPM to study the surface morphology and measure the root-mean-square (RMS) roughness. SPM images of the sol-gel-derived ZnO-based thin films deposited on glass substrates are presented in Figure 3. Those images show a uniformly granular morphology and dense surface. The significant differences between the three SPM images were the particle size and surface flatness. It was observed that the co-doped sample had the smallest particles and exhibited a flat surface morphology. The average particle sizes of the ZnO, ZnO:N, and ZnO:Ga–N thin films, as estimated from the corresponding 2D SPM images (Figure S2) in

ImageJ software, were 77.3, 46.2, and 39.3 nm, respectively. The observation of surface morphological characteristics of the thin film samples by SPM had a good agreement with the XRD results. Table 1 lists the values of RMS roughness of the ZnO, ZnO:N, and ZnO:Ga–N thin film samples, which were 3.6, 2.7, and 1.1 nm, respectively. As noted above, the impurity doping reduced the particle (crystallite) size and thereby decreased the surface roughness.

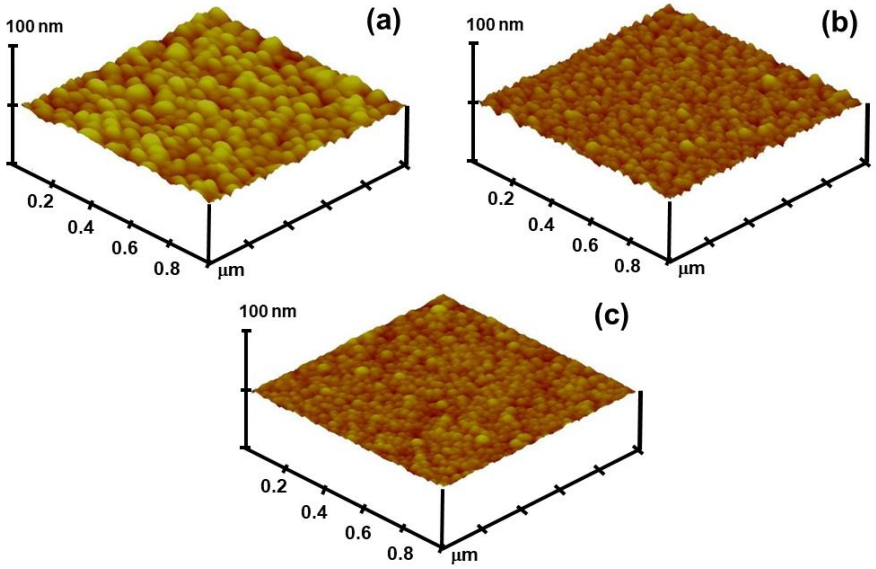

Figure 3. Three-dimensional (3D) scanning probe microscope (SPM) micrographs of the free surfaces of ZnO-based thin films: (**a**) undoped, (**b**) N-doped, and (**c**) Ga–N co-doped samples.

XPS examinations were performed to determine the elements responsible and identify the chemical bonding states of the ZnO-based thin films produced in this study. The narrow scan XPS spectra of Zn, O, and N regions of ZnO-based thin films are presented in Figure 4. The core level peaks of Zn 2*p* are presented in Figure 4a; they revealed similar XPS spectra for the three samples. The peaks of binding energies at 1021.0 and 1044.2 eV for the ZnO sample corresponded to the Zn $2p_{3/2}$ and Zn $2p_{1/2}$ components, respectively (spectrum (i) in Figure 4a). The electronic state of Zn $2p_{3/2}$ is associated with the Zn^{2+} ions in the ZnO lattice [7,28]. In addition, the Zn 2*p* XPS spectra of the two impurity-doped samples showed slight shifts toward the lower binding region due to changes in the strength of the metal–oxygen bond energy because of the incorporation of N and Ga–N dopants into the ZnO nanocrystals.

As shown in Figure 4b, the recorded O 1*s* spectra were obviously broad and asymmetric on the high binding energy side (solid lines). Each O 1*s* spectrum was deconvoluted to three distinct sub-curves (dashed lines) by Gaussian curve fitting and denoted with O_I, O_{II}, and O_{III} for representing three types of oxygen levels in oxide thin film samples [29,30]. The low binding energy component (O_I) exhibited the strongest intensity, was centered at 529.6 eV, and was associated with O^{2-} ions bonded with metal ions (Zn^{2+} and/or Ga^{3+}), such as Zn–O bonds, in the ZnO lattice. The component at the middle binding energy (O_{II}) was centered at 531.1 eV, usually associated with the loosely bound oxygen, and related to the oxygen vacancy concentration. The component at the high binding energy region (O_{III}), with a weak signal, was ascribed to chemisorbed or dissociated oxygen species, such as hydroxyl groups (–OH) bonded to the surfaces and/or the grain boundaries of the polycrystalline oxide films. The calculated O_{II}/O_{total} intensity ratios for the ZnO, ZnO:N, and ZnO:Ga–N nanostructured thin films were 20.44%, 21.30%, and 27.46%, respectively. Such intensity ratios are suggested for evaluating the relative concentrations of oxygen vacancies between the oxide thin film samples. The calculated results reveal that the co-doped ZnO thin film had a higher O_{II}/O_{total} ratio than those of the un-doped and single-doped ZnO thin films, indicating that weaker metal–oxygen bonds formed in the former sample than in the latter samples. The reduced strength in the metal–oxygen bonds can be attributed

to the Ga doping in ZnO:N crystals, which in turn led to a significant increase in the oxygen vacancy concentration in the ZnO:Ga–N thin film.

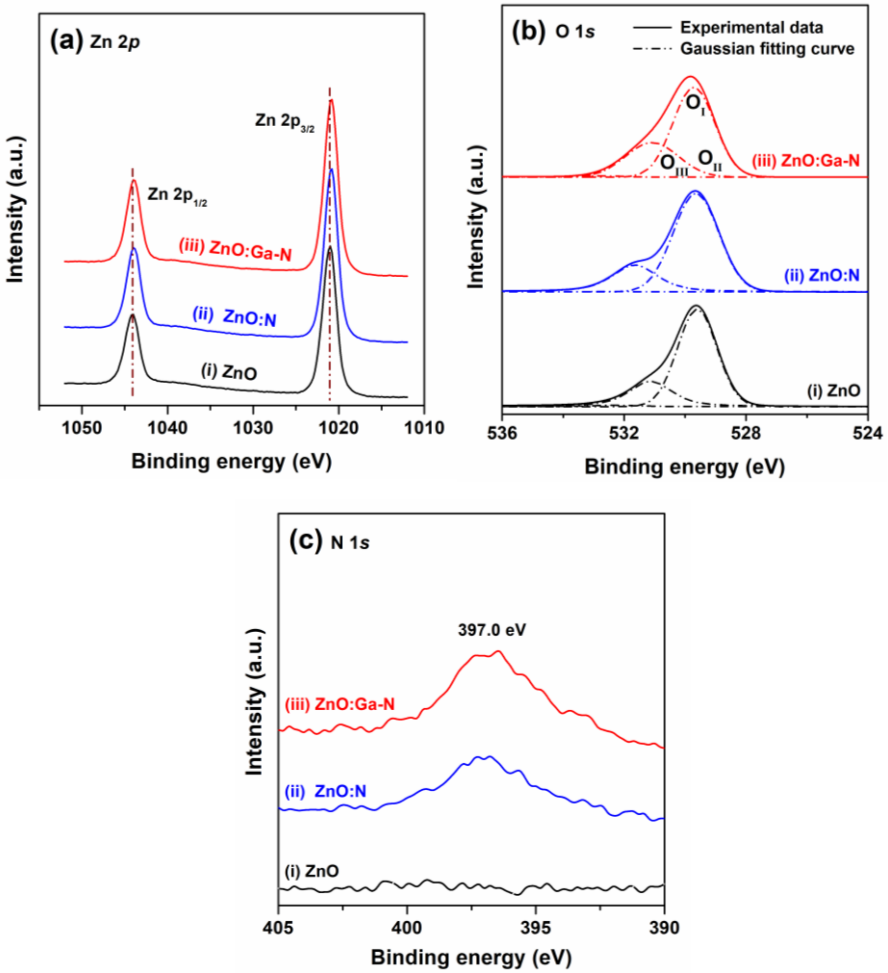

Figure 4. X-ray photoelectron spectroscopy (XPS) spectra of (**a**) Zn 2*p*, (**b**) O 1*s*, and (**c**) N 1*s* of the three ZnO-based thin films.

Figure 4c shows the N 1*s* XPS core level spectra and the single peak centered at about 397.0 eV, which was related to the formation of the No–Zn bond [23,31] and indicated that N ions were incorporated into the ZnO lattices of the N doped and Ga–N co-doped thin films. It was also demonstrated that Ga–N co-doping enhanced the solubility of the acceptor dopant (N) in ZnO nanocrystals (spectrum (iii) in Figure 4c. Ravichandran et al. suggested that the presence of N in the energy region, about 397.3 eV, is indicative of p-type conductivity [32]. In addition, the Ga 2*p* spectrum of the Ga–N co-doped sample is presented in Figure S3. The peak spectrum located at 1117.4 eV corresponds to the electrical state of Ga $2p_{3/2}$ and is ascribed to Ga^{3+} in gallium(III) oxide [33]. The actual contents of N and Ga + N in the ZnO:N and ZnO:Ga–N thin film samples were estimated by XPS analysis to be 0.52 at.%, and 1.1 at.% + 0.76 at.%. The examined results confirm that the N and Ga + N were successfully substituted into the ZnO nanocrystals and the solubility of desirable accept dopant (N) was enhanced through co-doping of Ga and N.

The effects on the optical characteristics of the incorporation N and Ga–N in ZnO thin films were investigated by optical transmission measurement. Figure 5a shows three typical optical transmittance spectra, which were recorded from the samples of glass/oxide thin films in the wavelength range of 200–1000 nm. These transmittance spectra exhibited high transparency (>85.0%) in the visible region and displayed an abrupt increase in absorption in the near-UV spectral range. The character of the optical absorption edge (band-edge absorption) is related to direct optical excitation from the valence

band to the conduction band and the magnitude of the bandgap energy. The slight shift toward the short wavelength region of the absorption edge in the two impurity-doped thin film samples may be associated with the finer microstructures.

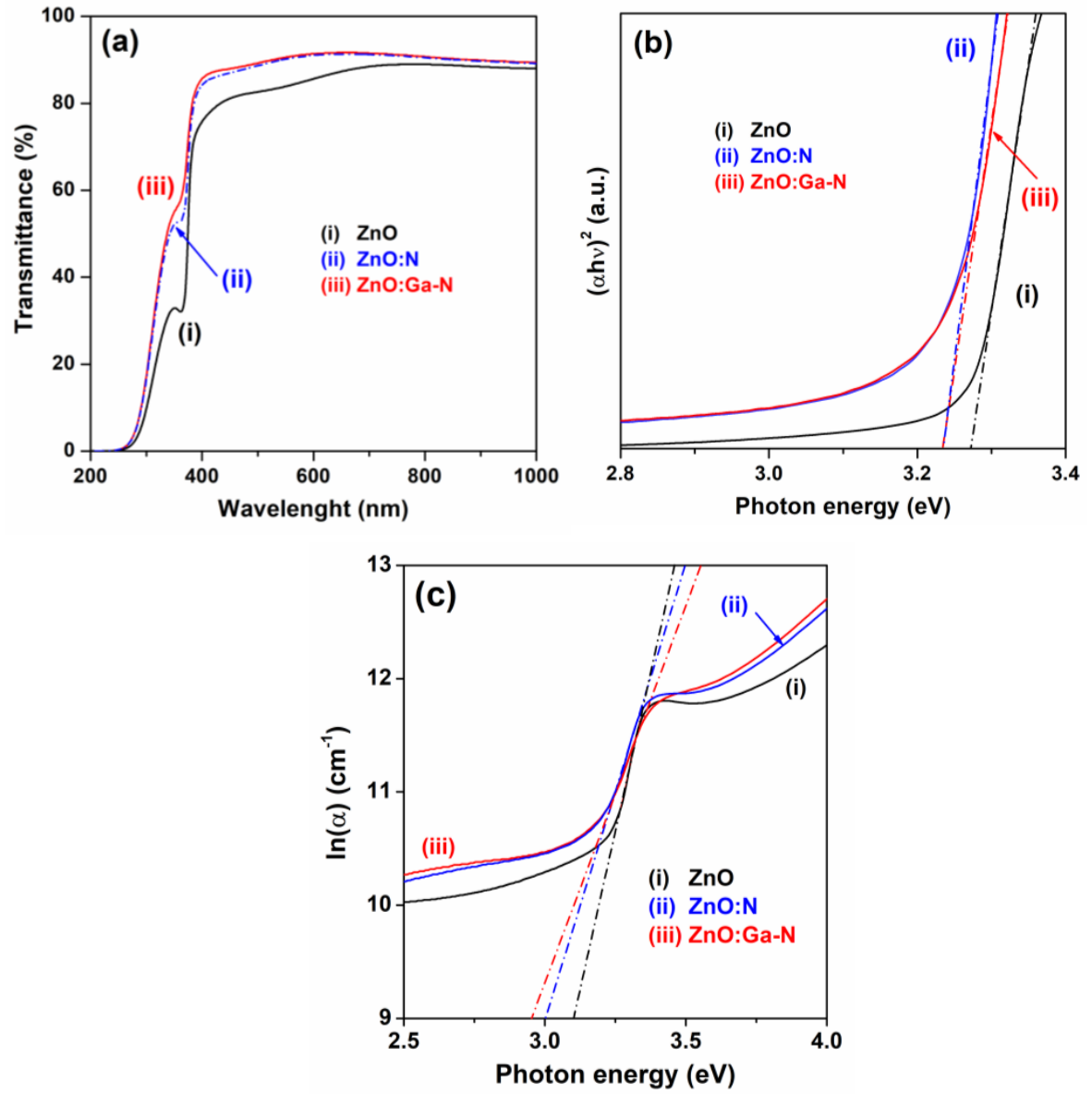

Figure 5. (**a**) Optical transmission spectra, (**b**) plot of $(\alpha h\nu)^2$ versus photo energy ($h\nu$), and (**c**) plot of $\ln(\alpha)$ versus photon energy ($h\nu$) of ZnO, ZnO:N, and ZnO:Ga–N thin film samples.

The recorded optical transmittance spectra indicated that the ZnO:N and ZnO:Ga–N samples exhibited a similar transmission characteristic and had higher transparency than the ZnO sample, covering the visible light region due to the former (impurity-doped samples) being thinner and having a flatter free surface (see Figures 2 and 3) compared with the latter (undoped sample). The average transmittances of undoped and impurity-doped ZnO thin film samples in the visible region (400 to 800 nm) were about 85.0% and approached 90.0% (the fourth column in Table 1). It is known that the optical transmittance of functional oxide thin films is strongly affected by film thickness, surface roughness, densification, crystallinity, and structural homogeneity.

The absorption coefficient (α), one of the intrinsic optical parameters of functional oxide films, can serve as a rough estimation from measured transmittance data with the Beer–Lambert law ($\alpha = [\ln(1/T)]/d_f$), where d_f is the thickness of the examined thin film sample, by assuming reflectance

to be negligible ($R = 0$). The calculated results are listed in Table 1. These results reveal that the average absorption coefficient of the undoped sample approached 1.9×10^4 cm^{-1} in the visible region and that an abrupt increase in the absorption coefficient (>26.3%) occurred in the two impurity-doped samples due to the microstructural changes and crystallinity degradation as well as impurity band formation. For optoelectronic materials, the relationship between the absorption coefficient (α) and optical bandgap (Eg) can be expressed as the following relation [34]:

$$\alpha(h\nu) = A\ (h\nu - E_g)^n \quad (1)$$

where h is Planck's constant, ν is the frequency of incident photons, the coefficient A is an energy-independent proportionality constant related to the band tailing states, and the exponent n varies according to the energy-band structure of the examined optoelectronic material. For direct allowed transitions, the value of n is 1/2. Figure 5b shows the plot of variation of $(\alpha h\nu)^2$ with the photon energy (eV) (namely, the Tauc plot), which was acquired from the optical transmittance spectra. A Tauc plot is used to determine the optical bandgap energy in semiconductors by extrapolating the straight-line portion near the onset of the absorption edge of the absorption curve to intercept the photon energy axis. The estimated optical bandgap energy of the impurity-doped ZnO thin films was 3.24 eV, which was slightly narrower than that of the undoped ZnO thin film (3.27 eV). Narrowing of the optical bandgap has been reported for ZnO:N, ZnO:Al–N, and ZnO:In–N thin films. That feature can be explained by the change in crystallite size and the formation of shallower impurity (acceptor and donor) states.

The Urbach energy (E_U) width has been considered for the study of the structural disorder and band-tail states of semiconductor thin films with impurity doping [22,35]. It can be estimated by the following expression [36]:

$$\alpha = \alpha_0 \exp(h\nu/E_U), \quad (2)$$

where α_0 is a constant. We determined the Urbach energy from the plot of ln (α) versus photo energy ($h\nu$) (Figure 5c) from the inverse of the slope of the linear segment of the optical absorption spectrum and found that the E_U values increased from 89.2 meV (ZnO) to 123.8 meV (ZnO:N) and 148.5 meV (ZnO:Ga–N). These changes demonstrated that the crystallinity degraded with increases in the dopant species.

Polycrystalline ZnO thin films exhibit strongly stimulated emissions through excitons even at room temperature, which is one of their unique optical properties [37]. Two emission signals appeared in each RT PL spectrum (Figure 6), including a sharp and intense UV emission peak centered at around 379 nm and a weak broad emission band in the visible region. The near-band-edge (NBE) UV emission is created by excitonic emission. A similar UV emission peak (380 nm) has been reported for ZnO thin films deposited on sapphire by sol-gel technique [32]. It is well known that the broad emission in the visible region is due to deep-level emission related to intrinsic defects such as Zn interstitials and O vacancies. It is worth noting that the decrease in the intensity of NBE emission after doping with N and Ga–N indicated the degeneration of the films' crystallinity and was ascribed to the increment of non-radiative recombination due to effects induces by N [22,24]. The N and Ga–N doping also led to a slight shift in the NBE emission peak as noted in the optical transmittance spectra in the near-UV spectral region. Moreover, the suppression of the visible emission may be attributed to the compensation of intrinsic defects by the acceptor dopants (spectra (ii) and (iii) in Figure 6). This feature confirmed the greater solubility and stability of the N dopant incorporated in the co-doped ZnO thin film.

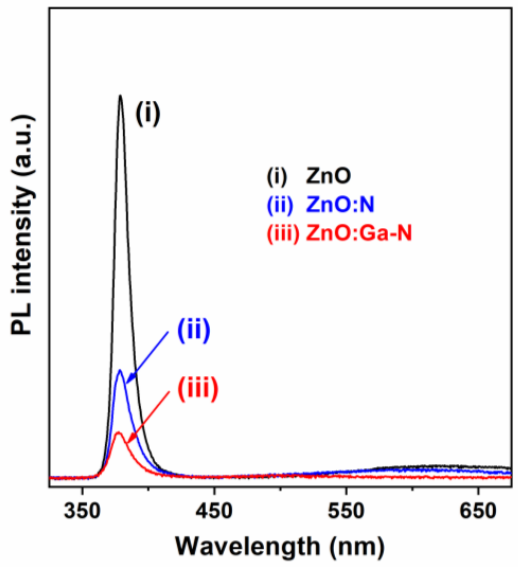

Figure 6. Comparison of the room-temperature photoluminescence (PL) spectra of ZnO, ZnO:N, and ZnO:Ga–N thin film samples.

Various electrical parameters, including the carrier type, carrier concentration, Hall mobility, and electrical resistivity, of the ZnO-based semiconductor thin films, measured by Hall-effect measurement, are presented in Table 2. It was confirmed that the pure ZnO thin films had n-type characteristics with a mean electron concentration of 3.19×10^{15} cm^{-3}, a mean carrier mobility of 20.77 $cm^2/V{\cdot}s$, and a mean resistivity of 94.32 $\Omega{\cdot}cm$. The measurement results also indicate that the as-prepared ZnO:N thin films exhibited a mean hole concentration of 1.83×10^{15} cm^{-3}, a mean hole mobility of 8.85 $cm^2/V{\cdot}s$, and a mean resistivity of 385.4 $\Omega{\cdot}cm$. This change in conductivity type from n to p was related to the incorporation of N dopant into ZnO, which induced shallow acceptors of N_O. However, the hole concentration and resistivity should be improved to achieve device-quality p-type oxide films. It is noted that the mean hole concentration of the p-type ZnO:Ga–N thin films approached 4.0×10^{17} cm^{-3}; this magnitude is comparable to those in previous reports on sol-gel-derived Al–N and In–N co-doped p-type ZnO thin films [22,24]. In addition, the mobility of the co-doped sample was only about 3.0 $cm^2/V{\cdot}s$, possibly due to the formation of the Ga–2N complex; this low mobility caused carrier scattering and restricted the hole mobility. Thus, the hole mobility of the p-type ZnO semiconductor thin films for device applications should be improved in future work.

Table 2. Electrical characteristics of the three ZnO-based thin films and the electrical stability of p-type ZnO:N and ZnO:Ga–N thin films.

Sample	Time of Measurement	Carrier Type *	Carrier Concent. (cm^{-3})	Mobility ($cm^2/V{\cdot}s$)	Resistivity ($\Omega{\cdot}cm$)
ZnO	As-deposited	n	-3.19×10^{15}	20.77	94.32
ZnO:N	As-deposited	p	1.83×10^{15}	8.85	385.4
	After 14 days	p	5.21×10^{14}	7.53	1.59×10^{3}
	After 21 days	n	-2.47×10^{14}	7.87	3.21×10^{3}
	After 28 days	n	-7.04×10^{13}	7.42	1.19×10^{4}
ZnO:Ga–N	As-deposited	p	3.96×10^{17}	3.10	5.09
	After 14 days	p	7.52×10^{16}	2.31	36.0
	After 21 days	p	2.28×10^{16}	2.05	133.5
	After 28 days	n	-3.92×10^{15}	4.18	380.9

* The symbols of n and p represent the type of major carrier concentration. (n: electron and p: hole).

Ye et al. summarized the electrical properties of several types of group III (B, Al, Ga, and In)–N co-doped p-type ZnO thin films and found that the hole concentration density, Hall mobility, and electrical resistivity were in the ranges of 3×10^{16} to 5×10^{18} cm^{-3}, 0.1 to 15 $cm^2/V{\cdot}s$, and 0.015

to 2×10^2 Ω·cm, respectively [7]. The main considerations of the acceptor-donor co-doping method for achieving p-type conduction in ZnO thin films are to lower the ionization energy of acceptors and donors, enhance the solubility of acceptor dopants [38], and reduce the self-compensation effect to create shallower acceptor levels (falling within the range of 0.1–0.2 eV above the valence-band maximum (VBM)).

For verification of the electrical stability of the p-type oxide thin films, the electrical characteristics were measured in time frames of two to four weeks with periods of 7 days (Table 2). We found that these p-type ZnO:N thin films reverted to n-type over time. The Ga–N co-doped ZnO thin films exhibited more stable p-type conductivity at 3 weeks than did the N-doped ZnO thin films (<three weeks) due to the formation of the Ga_{Zn}–N_O pairs, which could offer more efficient incorporation of N dopants and activation of acceptors, and hence the creation of impurity bands above the VBM of ZnO, which increased the hole concentration. A comparison of the electrical characteristics in previous reports on solution-processed group III element (B, Al, In, and Ga)–N co-doped p-type ZnO thin films with those of the developed ZnO:Ga–N thin films in this work is provided in Table 3. It was found that the electrical properties of ZnO-based thin films fabricated by spray pyrolysis technique are better than those of oxide films prepared by sol-gel process.

Table 3. Comparison of the electrical characteristics of solution-processed group III elements-N co-doped p-type ZnO thin films with the developed ZnO:Ga–N thin film in this study.

Dopant	Method	Hole Concent. (cm^{-3})	Mobility ($cm^2/V{\cdot}s$)	Resistivity (Ω·cm)	Stability	Ref.
B–N	Spray pyrolysis	5.89×10^{18}	12.86	8.54×10^{-2}	20 days	[18]
Al–N	Spray pyrolysis	2.30×10^{18}	0.94	2.89	-	[28]
Al–N	Sol-gel	2.0×10^{17}	1.6	19.0	-	[24]
Al–N	Sol-gel	8.11×10^{16}	9.97	77.0	-	[14]
In–N	Spray pyrolysis	2.0×10^{19}	3.0	7.70×10^{-2}	30 days	[38]
In–N	Sol-gel	9.81×10^{17}	0.60	1.58×10^{-1}	-	[22]
Ga–N	Spray pyrolysis	3.82×10^{19}	4.34	3.97×10^{-2}	30 days	[19]
Ga–N	Sol-gel	3.96×10^{17}	3.10	5.09	>21 days	This work

The authors examined the optical and electrical properties of the three kinds of sol-gel-derived ZnO-based thin films and connected them with the structural characteristics. Besides comparing the physical properties of the oxide thin films, our experimental investigations clarified the stability of p-type ZnO:N and ZnO:Ga–N thin films. Our study indicates that the p-type ZnO:Ga–N semiconductor thin films exhibited good electrical stability, without significant degeneration of the electrical characteristics, for at least three weeks. We have successfully fabricated Ga–N co-doped ZnO transparent semiconductor thin film, which may be applicable as a stable p-type layer in the development of ZnO-based homojunction or heterojunction electronic and optoelectronic devices.

4. Conclusions

Electrically stable p-type ZnO transparent semiconductor thin films have been deposited on alkali-free glass substrates with Ga and N co-doping by the sol-gel spin-coating process. XRD patterns showed that these sol-gel-derived ZnO-based thin films were polycrystalline with a single hexagonal structure, and the microstructural features were significantly changed by the impurity doping. XPS analysis confirmed the incorporation of N and Ga–N into the two kinds of impurity-doped thin films and demonstrated that Ga and N co-doping enhanced the solubility of N dopant in ZnO thin films. The N-doped and Ga–N co-doped ZnO thin films both exhibited high transparency (~90%) in the visible spectrum. It was confirmed that the nature of conductivity of ZnO semiconductor thin films changed from n-type to p-type when the N dopant was incorporated in the ZnO nanocrystals. In the present study, we succeeded in realizing good conductivity in p-type ZnO thin film through simultaneous co-doping of Ga and N, achieving a hole concentration of 3.96×10^{17} cm^{-3}, mobility of 3.1 $cm^2/V{\cdot}s$, and resistivity of 5.09 Ω·cm. The p-ZnO:Ga–N transparent semiconductor thin films exhibited electrical stability for almost four weeks.

Supplementary Materials: The following are available online at http://www.mdpi.com/2079-6412/10/11/1069/s1, Figure S1: Plane-view FE-SEM micrographs of ZnO-based thin films: (a) undoped, (b) N-doped, and (c) Ga–N co-doped samples, Figure S2: 2D SPM images of ZnO-based thin film surfaces: (a) undoped, (b) N-doped, and (c) Ga–N co-doped samples, Figure S3: Core level XPS spectrum of Ga 2*p* of the Ga–N co-doped ZnO thin film.

Author Contributions: Conceptualization, C.-Y.T. and W.-Y.C.; methodology, C.-Y.T. and W.-Y.C.; investigation and resources, C.-Y.T.; data curation, C.-Y.T. and W.-Y.C.; writing—original draft preparation and writing—review and editing, C.-Y.T.; project administration, C.-Y.T. All authors have read and agreed to the published version of the manuscript.

Funding: This research received no external funding.

Acknowledgments: The authors gratefully acknowledge the Precision Instrument Support Center of Feng Chia University for providing XRD, FE-SEM, and SPM characterization facilities and the Instrument Center of National Chung Hsing University, Taichung, Taiwan, for help with the XPS measurement.

Conflicts of Interest: The authors declare that there are no known conflict of interest associated with this publication and there is no significant financial support for this study that could have influenced its outcome.

References

1. Özgür, Ü.; Hofstetter, D.; Morkoç, H. ZnO devices and applications: A review of current status and future prospects. *Proc. IEEE* **2010**, *98*, 1255–1268. [CrossRef]
2. Özgür, Ü.; Alivov, Y.I.; Liu, C.; Teke, A.; Reshchikov, M.A.; Doğan, S.; Avrutin, V.; Cho, S.J.; Morkoç, A.H. A comprehensive review of ZnO materials and devices. *J. Appl. Phys.* **2005**, *98*, 041301. [CrossRef]
3. Wang, Z.; Nayak, P.K.; Caraveo-Frescas, J.A.; Alshareef, H.N. Recent developments in p-type oxide semiconductor materials and devices. *Adv. Mater.* **2016**, *28*, 3831–3892. [CrossRef] [PubMed]
4. Yadav, H.M.; Otari, S.V.; Bohara, R.A.; Mali, S.S.; Pawar, S.H.; Delekar, S.D. Synthesis and visible light photocatalytic antibacterial activity of nickel-doped TiO_2 nanoparticles against Gram-positive and Gram-negative bacteria. *J. Photochem. Photobiol. A Chem.* **2014**, *294*, 130–136. [CrossRef]
5. Shang, Z.-W.; Hsu, H.-H.; Zheng, Z.-W.; Cheng, C.-H. Progress and challenges in p-type oxide-based thin film transistors. *Nanotechnol. Rev.* **2019**, *8*, 422–443. [CrossRef]
6. Zhang, S.B.; Wei, S.-H.; Zunger, A. Intrinsic n-type versus p-type doping asymmetry and the defect physics of ZnO. *Phys. Rev. B* **2001**, *63*, 075205. [CrossRef]
7. Ye, Z.; He, H.; Jiang, L. Co-doping: An effective strategy for achieving stable p-type ZnO thin films. *Nano Energy* **2018**, *52*, 527–540. [CrossRef]
8. Yan, Y.; Li, J.; Wei, S.-H.; Al-Jassim, M.M. Possible approach to overcome the doping asymmetry in wideband gap semiconductors. *Phys. Rev. Lett.* **2007**, *98*, 135506. [CrossRef]
9. Janotti, A.; Van De Walle, C.G. Fundamentals of zinc oxide as a semiconductor. *Rep. Prog. Phys.* **2009**, *72*, 126501. [CrossRef]
10. Tsay, C.-Y.; Lee, W.-C. Effect of dopants on the structural, optical and electrical properties of sol–gel derived ZnO semiconductor thin films. *Curr. Appl. Phys.* **2013**, *13*, 60–65. [CrossRef]
11. Duan, X.M.; Stampfl, C.; Bilek, M.M.M.; McKenzie, D.R. Codoping of aluminum and gallium with nitrogen in ZnO: A comparative first-principles investigation. *Phys. Rev. B* **2009**, *79*, 235208. [CrossRef]
12. Look, D.C.; Claflin, B.; Alivov, Y.I.; Park, S.J. The future of ZnO light emitters. *Phys. Status Solidi* **2004**, *201*, 2203–2212. [CrossRef]
13. Park, C.H.; Zhang, S.B.; Wei, S.-H. Origin of p-type doping difficulty in ZnO: The impurity perspective. *Phys. Rev. B* **2002**, *66*, 073202. [CrossRef]
14. Saravanakumar, B.; Mohan, R.; Thiyagarajan, K.; Kim, S.-J. Investigation of UV photoresponse property of Al, N co-doped ZnO film. *J. Alloys Compd.* **2013**, *580*, 538–543. [CrossRef]
15. Yamamoto, T.; Katayama-Yoshida, H. Solution using a codoping method to unipolarity for the fabrication of p-type ZnO. *Jpn. J. Appl. Phys.* **1999**, *38*, L166–L169. [CrossRef]
16. Joseph, M.; Tabata, H.; Kawai, T. p-type electrical conduction in ZnO thin films by Ga and N codoping. *Jpn. J. Appl. Phys.* **1999**, *38*, L1205–L1207. [CrossRef]
17. Li, W.; Kong, C.; Qin, G.; Ruan, H.; Fang, L. p-type conductivity and stability of Ag–N codoped ZnO thin films. *J. Alloys Compd.* **2014**, *609*, 173–177. [CrossRef]
18. Narayanan, N.; Deepak, N. B–N codoped p type ZnO thin films for optoelectronic applications. *Mater. Res.* **2018**, *21*, 20170618. [CrossRef]

19. Narayanan, N.; Deepak, N. Melioration of optical and electrical performance of Ga–N codoped ZnO thin films. *Z. Für Nat. A* **2018**, *73*, 547–553. [CrossRef]
20. Lu, J.G.; Ye, Z.Z.; Zhuge, F.; Zeng, Y.-J.; Zhao, B.H.; Zhu, L.P. p-type conduction in N–Al co-doped ZnO thin films. *Appl. Phys. Lett.* **2004**, *85*, 3134. [CrossRef]
21. Matsui, H.; Saeki, H.; Tabata, H.; Kawai, T. Role of Ga for Co-doping of Ga with N in ZnO films. *Jpn. J. Appl. Phys.* **2003**, *42*, 5494–5499. [CrossRef]
22. Cao, Y.; Miao, L.; Tanemura, S.; Tanemura, M.; Kuno, Y.; Hayashi, Y. Low resistivity p-ZnO films fabricated by sol-gel spin coating. *Appl. Phys. Lett.* **2006**, *88*, 251116. [CrossRef]
23. Bian, J.M.; Li, X.M.; Gao, X.D.; Yu, W.D.; Chen, L.D. Deposition and electrical properties of N–In codoped p-type ZnO films by ultrasonic spray pyrolysis. *Appl. Phys. Lett.* **2004**, *84*, 541–543. [CrossRef]
24. Dutta, M.; Ghosh, T.; Basak, D. N doping and Al–N co-doping in sol-gel ZnO films: Studies of their structural, electrical, optical, and photoconductive properties. *J. Electron. Mater.* **2009**, *38*, 2335–2342. [CrossRef]
25. Janotti, A.; Van De Walle, C.G. Oxygen vacancies in ZnO. *Appl. Phys. Lett.* **2005**, *87*, 122102. [CrossRef]
26. Tsay, C.-Y.; Hsu, W.-T. Comparative studies on ultraviolet-light-derived photoresponse properties of ZnO, AZO, and GZO transparent semiconductor thin films. *Materials* **2017**, *10*, 1379. [CrossRef]
27. Tsay, C.-Y.; Fan, K.-S.; Lei, C.-M. Synthesis and characterization of sol-gel derived gallium-doped zinc oxide thin films. *J. Alloys Compd.* **2012**, *512*, 216–222. [CrossRef]
28. Zhang, X.; Fan, H.; Sun, J.; Zhao, Y. Structural and electrical properties of p-type ZnO films prepared by ultrasonic spray pyrolysis. *Thin Solid Films* **2007**, *515*, 8789–8792. [CrossRef]
29. Park, G.C.; Hwang, S.M.; Lee, S.M.; Choi, J.H.; Song, K.M.; Kim, H.Y.; Eum, S.-J.; Jung, S.-B.; Lim, J.H.; Joo, J. Hydrothermally grown In-doped ZnO nanorods on p-GaN films for color-tunable heterojunction light-emitting-diodes. *Sci. Rep.* **2015**, *5*, 10410. [CrossRef]
30. Futsuhara, M.; Yoshioka, K.; Takai, O. Structural, electrical and optical properties of zinc nitride thin films prepared by reactive rf magnetron sputtering. *Thin Solid Films* **1998**, *322*, 274–281. [CrossRef]
31. Zhang, J.P.; Zhang, L.D.; Zhu, L.Q.; Zhang, Y.; Liu, M.; Wang, X.J.; He, G. Characterization of ZnO:N films prepared by annealing sputtered zinc oxynitride films at different temperatures. *J. Appl. Phys.* **2007**, *102*, 114903. [CrossRef]
32. Ravichandran, C.; Srinivasan, G.; Lennon, C.; Sivanathan, S.; Kumar, J. Investigations on the structural and optical properties of Li, N and (Li, N) co-doped ZnO thin films prepared by sol-gel technique. *Mater. Sci. Semicond. Process.* **2010**, *13*, 46–50. [CrossRef]
33. Rakhshani, A.E.; Bumajdad, A.; Kokaj, J.; Thomas, S. Structure, composition and optical properties of ZnO:Ga films electrodeposited on flexible substrates. *Appl. Phys. A* **2009**, *97*, 759–764. [CrossRef]
34. Huang, K.; Tang, Z.; Zhang, L.; Yu, J.; Lv, J.; Liu, X.; Liu, F. Preparation and characterization of Mg-doped ZnO thin films by sol-gel method. *Appl. Surf. Sci.* **2012**, *258*, 3710–3713. [CrossRef]
35. Melsheimer, J.; Ziegler, D. Band gap energy and Urbach tail studies of amorphous, partially crystalline and polycrystalline tin dioxide. *Thin Solid Films* **1985**, *129*, 35–47. [CrossRef]
36. Mia, M.N.H.; Pervez, M.F.; Hossain, M.K.; Rahman, M.R.; Uddin, M.J.; Al Mashud, M.A.; Ghosh, H.K.; Hoq, M. Influence of Mg content on tailoring optical bandgap of Mg-doped ZnO thin film prepared by sol-gel method. *Results Phys.* **2017**, *7*, 2683–2691. [CrossRef]
37. Ryu, Y.R.; Zhu, S.; Look, D.C.; Wrobel, J.M.; Jeong, H.M.; White, H.W. Synthesis of p-type ZnO films. *J. Cryst. Growth* **2000**, *216*, 330–334. [CrossRef]
38. Yu, C.-C.; Lan, W.-H.; Huang, K.-F. Indium-nitrogen codoped zinc oxide thin film deposited by ultrasonic spray pyrolysis on n-(111) Si substrate: The effect of film thickness. *J. Nanomater.* **2014**, *2014*, 1–7. [CrossRef]